FACTA UNIVERSITATIS
Series: **Mechanical Engineering** Vol. 12, N^{o} 3, 2014, pp. 305 - 323

EFFECT OF VARIOUS POROUS STRUCTURES ON THE SHLIOMIS MODEL BASED FERROFLUID LUBRICATION OF THE FILM SQUEEZED BETWEEN ROTATING ROUGH CURVED CIRCULAR PLATES

UDC532:621.8

Jimit R. Patel, Gunamani Deheri

Department of Mathematics, Sardar Patel University

Abstract: *Efforts have been made to analyze the Shliomis model based ferrofluid lubrication of a squeeze film between rotating rough curved circular plates where the upper plate has a porous facing. Different models of porosity are treated. The stochastic modeling of Christensen and Tonder has been employed to evaluate the effect of surface roughness. The related stochastically averaged Reynolds type equation is numerically solved to obtain the pressure distribution, leading to the calculation of load carrying capacity. The results presented in graphical form establish that the Kozeny-Carman model is more favorable as compared to the Irmay one from the design point of view. It is observed that the Shliomis model based ferrofluid lubrication performs relatively better than the Neuringer-Rosensweig one. Although the bearing suffers due to transverse surface roughness, with a suitable choice of curvature parameters and rotational ratio, the negative effect of porosity and standard deviation can be minimized by the ferrofluid lubrication at least in the case of negatively skewed roughness.*

Key Words: *Squeeze Film, Curved Circular Plates, Roughness, Magnetic Fluid, Rotation, Porous Structures*

1. INTRODUCTION

Wu [1] has analyzed the effect of rotation on the squeeze film performance in porous circular disks. The criteria for neglecting the inertia effects are laid down in this study.

Murti [2] has discussed the squeeze film behavior between the porous circular disks when the upper disk had a porous facing. By means of the Fourier Bessel's series the equation for pressure distribution is derived. It is shown that the enhanced value of permeability parameter has diminished pressure over the entire disk. Vora and Bhat [3]

Received: September 3, 2014.
Corresponding author: Jimit R Patel
Department of Mathematics, Sardar Patel University, Vallabh Vidyanagar, Anand,Gujarat India-388120.
E-mail: patel.jimitphdmarch2013@gmail.com

have obtained the load carrying capacity of a squeeze film between the curved porous rotating circular plates. The effect of the rotating fluid inertia reduces the load carrying capacity significantly. Paras ram and Vikaskumar [4] have examined the effects of magnetic field dependent viscosity on the steady axi-symmetric ferrofluid flow due to the rotating disk in a porous medium.

Verma [5] has investigated the magnetic fluid lubrication effect of a squeeze film between two approaching surfaces in the presence of an externally applied magnetic field, oblique to the lower surfaces. The magnetization effects induce enhanced load carrying capacity and longer squeeze time. Lu et al. [6] have evaluated the effects of fluid inertia in magneto hydrodynamic annular squeeze films. It is observed that the inertia correction factor in the magneto-hydrodynamic load carrying capacity is more pronounced with large Hartmann numbers. Hsu et al. [7] have studied the magneto- hydrodynamic squeeze film behavior between circular disks by taking rotational inertial effects into consideration. It is established that the overall squeeze film performance characteristics of rotating circular disks are improved when using an electrically conducting fluid in the presence of a transverse magnetic field. Zueco and Beg [8] have numerically analyzed the hydromagnetic squeeze film flow between two parallel rotating circular disks with induced magnetic field. This study finds applications in hydro magnetic lubrication of breaking devices and rotating machinery. Huang et al. [9] have experimentally studied the ferrofluid lubrication with an external magnetic field. With an appropriate magnetic field the load carrying capacity is significantly enhanced. Patel and Deheri [10] have analyzed the effect of various porous structures on the performance of a Shliomis model based ferrofluid lubrication of the film squeezed in rotating rough porous curved circular plates. It is found that by suitably choosing curvature parameters and rotational inertia, the adverse effect of transverse roughness could be overcome by the positive effect of ferrofluid lubrication in the case of negatively skewed roughness when the Kozeny-Carman model is deployed.

Ting [11] has considered the fluid inertia effects to develop a mathematical analog of determination of porous annular disk squeeze film behavior. It is concluded that the inertia effect results in decreased load carrying capacity and reduced squeeze time. A review of the performance of porous squeeze films between lubricated plates is presented by Wu [12]. Bhat and Deheri [13] have dealt with the squeeze film behavior in porous annular disks lubricated with a magnetic fluid. The load carrying capacity rose sharply with increasing magnetization. Bhat and Deheri [14] have theoretically analyzed magnetic fluid based squeeze film in curved porous circular disks. The pressure, load carrying capacity and the response time are found to increase with increasing magnetization. However, the effects due to magnetization are independent of the upper plate's curvature. Elsharkawy and Nassar [15] have discussed the hydrodynamic lubrication of porous squeeze film bearing. The increase in the permeability parameter causes decreased load carrying capacity. Gupta and Deheri [16] investigate the effect of surface roughness on the behavior of squeeze film in a spherical bearing. It is shown that the performance of the bearing system is adversely affected by the composite roughness of the surfaces. Deheri et al. [17] have analyzed the magnetic fluid lubrication of a squeeze film between transversally rough curved plates. In this case it is established that the combined effect of magnetization and curvature parameters leads to an increased load carrying capacity although the effect of standard deviation is adverse in general. Basti [18] has studied the combined effect of couple stress and surface roughness on the performance of the film

squeezed between curved annular plates. Performance of the squeeze film suffer due to radial roughness pattern. However, circumferential roughness pattern improves the squeeze film characteristics for couple stress lubrication.

Prakash and Tiwari [19] consider the surface roughness effect on the response of a squeeze film between two circular plates one with porous facing. Deheri et al. [20] analyze the performance of a magnetic fluid based squeeze film between porous circular plates considering porous matrix of variable film thickness. A significant observation is that with a proper selection of thickness ratio parameter, a magnetic fluid based squeeze film bearing with variable thickness could be made to perform considerably better than that of a conventional porous bearing with a uniform porous matrix thickness working with a conventional lubricant. Vadher et al. [21] have discussed the behavior of hydro magnetic squeeze films between conducting rough porous circular plates. With a suitable choice of the conductivity parameter the negatively skewed roughness induces load carrying capacity further enhanced significantly owing to magnetization. Lastly, Patel and Deheri [22] analyze the performance of a ferrofluid based squeeze film in rotating rough curved circular plates resorting to Shliomis model. Recently, Patel and Deheri [23] have investigated the effect of different porous structures on the performance of a Shliomis model based magnetic squeeze film in rotating rough porous curved circular plates. The results presented in graphical form show that the adverse effect of transverse roughness could be compensated by a positive effect of magnetization in the case of negatively skewed roughness, a suitable choice of the rotation ratio and of curvature parameters. It is also found that this compensation appears to be more in the case of the Kozeny-Carman model as compared to that of Irmay one.

This paper tends to analyze the effect of various porous structures on the Shliomis model based ferrofluid lubrication of a squeeze film between the curved rough rotating circular plates with the upper one having a porous facing.

2. ANALYSIS

The configuration of the curved circular bearing is given in Fig. 1. Here the bearing consists of two plates, each of radiuses a. The lower and upper plates rotate with angular velocities Ω_l and Ω_u respectively, about the z-axis. The upper disk moves normally towards the lower disk with uniform velocity $\dot{h}_0$.

According to the discussion of Christensen and Tonder [24-26] the stochastic modeling of transverse roughness, film thickness h of the lubricant film is considered to be:

$$h = \bar{h} + h_s \tag{1}$$

where $\bar{h}$ is the mean film thickness and h_s is the deviation from the mean film thickness characterizing the random roughness of the bearing surfaces. Deviation h_s is derived by the probability density function:

$$f(h_s) = \begin{cases} \dfrac{35}{32c^7}(c^2 - h_s^2)^3, -c \le h_s \le c \\ 0, elsewhere \end{cases} \tag{2}$$

where c is the maximum deviation from the mean film thickness. The details regarding mean α, standard deviation σ and parameter ε which is the measure of symmetry of random variable h_s, are taken from the Christensen and Tonder's study [24-26].

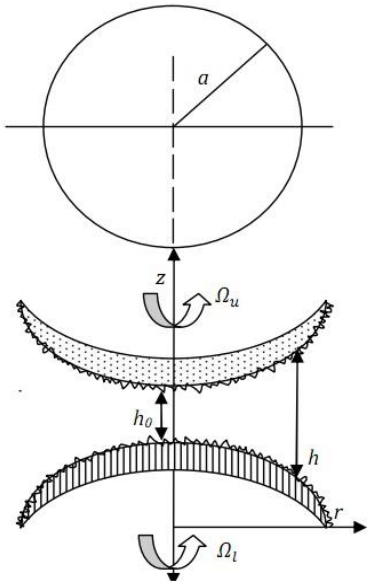

Fig. 1 Configuration of the bearing system

In view of the discussions of Bhat [27] and Abhangi and Deheri [28], it is assumed that the rotating upper plate lying along the surface determined by the relation:

$$z_u = h_0 \exp(-\beta r^2); 0 \le r \le a \tag{3}$$

approaches with normal velocity $\dot{h}_0$ to the rotating lower plate lying along the surface given by:

$$z_l = h_0[\exp(-\gamma r^2) - 1]; 0 \le r \le a \tag{4}$$

where β and γ are curvature parameters of the corresponding plates and h_0 is the central film thickness. Film thickness $h(r)$ is defined by (Bhat [27], Abhangi and Deheri [28]):

$$h(r) = h_0[\exp(-\beta r^2) - \exp(-\gamma r^2) + 1]; 0 \le r \le a \tag{5}$$

Shliomis [29] has established that magnetic particles of a magnetic fluid can relax in two ways when the applied magnetic field changes. The first is by the magnetic particles' rotation in the fluid and the second by rotation of the magnetic moment in the particles. Brownian relaxation time parameter τ_B gives particle rotation while relaxation time parameter τ_S describes the intrinsic rotational process. Assuming a steady flow and neglecting inertial and second derivatives of $\bar{S}$, the equations governing the flow become:

$$-\nabla_p + \eta\nabla^2\bar{q} + \mu_0(\overline{M}.\nabla)\overline{H} + \frac{1}{2\tau_s}\nabla\times(\bar{S} - I\overline{\Omega}) = 0 \tag{6}$$

$$\bar{S} = I\overline{\Omega} + \mu_0\tau_s(\overline{M}\times\overline{H}) \tag{7}$$

$$\overline{M} = M_0\frac{\overline{H}}{H} + \frac{\tau_B}{I}(\bar{S}\times\overline{M}) \tag{8}$$

where $\bar{S}$ is the internal angular momentum, I is the sum of moments of inertia of the particles per unit volume, $\overline{\Omega} = \frac{1}{2}\nabla\times\bar{q}$, together with:

$$\nabla.\bar{q} = 0, \nabla\times\overline{H} = 0, \nabla.(\overline{H} + \overline{M}) = 0 \tag{9}$$

(Bhat [27]), $\bar{q}$ is the fluid viscosity in the film region, $\overline{H}$ is external magnetic field, $\bar{\mu}$ is magnetic susceptibility of the magnetic field, p is the film pressure, η is the fluid viscosity and μ_0 is the permeability of the free space.

By making use of Eq. (7), in Eqs. (6) and (8), one finds that:

$$-\nabla_p + \eta\nabla^2\bar{q} + \mu_0(\overline{M}.\nabla)\overline{H} + \frac{1}{2}\mu_0\nabla\times(\overline{M}\times\overline{H}) = 0 \tag{10}$$

and

$$\overline{M} = M_0\frac{\overline{H}}{H} + \tau_B(\overline{\Omega}\times\overline{M}) \tag{11}$$

Neglecting $\tau_B\tau_s$ terms, substitution of $\overline{M}$ in above equation, leads to:

$$\begin{aligned}&-\nabla_p + (\eta + \frac{\mu_0}{4}\tau_B\overline{M}.\overline{H})\nabla^2\bar{q} + \mu_0(\overline{M}.\nabla)\overline{H}\\ &+\frac{1}{2}\mu_0\tau_B[\nabla(\overline{\Omega}.\overline{H})\times\overline{M} + (\overline{\Omega}..\overline{H}).\nabla\times\overline{M} - \nabla(\overline{M}.\overline{H})\times\overline{\Omega}] = 0\end{aligned} \tag{12}$$

From Eq. (11), it is easily observed that an initial approximation to $\overline{M}$ is:

$$\overline{M} = M_0\frac{\overline{H}}{H} \tag{13}$$

Substituting the value of $\overline{M}$ on the right side of Eq. (11), a second approximation to $\overline{M}$ is found to be:

$$\overline{M} = M_0\frac{\overline{H}}{H} + \frac{M_0}{H}\tau_B(\overline{\Omega}\times\overline{M}) \tag{14}$$

Again, substituting this value of $\overline{M}$ on the right side of Eq. (11), third approximation to $\overline{M}$ is availed as:

$$\overline{M}.\overline{H} = M_0H + \frac{M_0}{H}\tau_B^2[(\overline{\Omega}.\overline{H})^2 - \Omega^2H^2] \tag{15}$$

In view of the equations of Shliomis model in cylindrical polar coordinates with a uniform magnetic field, when both surfaces are solid and the upper one rotates, the governing equation for the film pressure is obtained as (Bhat [27]):

$$\frac{1}{r}\frac{d}{dr}\left((h^3+12\psi l_1)r\frac{dp}{dr}\right)=12\eta_a\dot{h}_0+24\rho\psi l_1\Omega_u^2+\frac{3}{10}\rho\Omega_u^2\frac{1}{r}\frac{d}{dr}(r^2h^3)+\frac{3}{320}\frac{N\tau_B^3}{\eta_a^3}\frac{1}{r}\frac{d}{dr}$$

$$\left[h^5r\left\{-\left(\frac{dp}{dr}\right)^3+\frac{27}{616}\rho^3r^3\Omega_u^6+\frac{13}{14}\left(\frac{dp}{dr}\right)^2\rho r\Omega_u^2-\frac{251}{756}\frac{dp}{dr}\rho^2r^2\Omega_u^4\right\}\right] \tag{16}$$

with l_1 being layer thickness.

Neglecting τ_B^3 term, following the discussions of Christensen and Tonder [24-26] regarding the modeling of roughness and under the usual assumptions of hydro-magnetic lubrication (Bhat [27], Prajapati [30], Deheri et al. [31]) the modified Reynolds equation when both plates rotate, takes the form:

$$\begin{aligned}\frac{1}{r}\frac{d}{dr}\left((g(h)+12\psi l_1)r\frac{dp}{dr}\right)&=12\eta(1+\tau)\dot{h}_0+24\rho\psi l_1\Omega_u^2\\&+\rho\left(\frac{3}{10}\Omega_r^2+\Omega_r\Omega_l+\Omega_l^2\right)\frac{1}{r}\frac{d}{dr}(r^2g(h))\end{aligned} \tag{17}$$

where.

$$g(h)=h^3+3h^2\alpha+3(\sigma^2+\alpha^2)h+3\sigma^2\alpha+\alpha^3+\varepsilon$$

The following non-dimensional quantities are considered:

$$\bar{h}=\frac{h}{h_0}=[\exp(-BR^2)-\exp(-CR^2)+1],R=\frac{r}{a},P=-\frac{h_0^3p}{\eta a^2\dot{h}_0},B=\beta a^2,$$

$$C=\gamma a^2,\bar{\sigma}=\frac{\sigma}{h_0},\bar{\alpha}=\frac{\alpha}{h_0},\bar{\varepsilon}=\frac{\varepsilon}{h_0^3},\eta_a=\eta(1+\tau),\Omega_r=\Omega_u-\Omega_l,S=-\frac{\rho\Omega_u^2h_0^3}{\eta\dot{h}_0},$$

$$\Omega_f=\frac{\Omega_l}{\Omega_u},l^*=\frac{l}{\bar{l}},\bar{\psi}=\frac{D_c^2l_1}{h_0^3},\psi^*=\frac{D_s^2l_1}{h_0^3},A=\frac{\bar{\psi}l^*e^3}{6(1-e)^2},D=\frac{\psi^*\left(1-(1-e)^{\frac{2}{3}}\right)}{(1-e)} \tag{18}$$

The related boundary conditions are:

$$P(1)=0,\left(\frac{dP}{dR}\right)_{R=0}=0 \tag{19}$$

2.1 A globular sphere model

A porous material is filled with globular spherical particles (mean particle size D_C) as shown in Fig. 2.

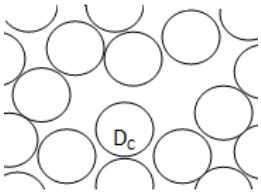

Fig. 2 Structure model of porous sheets given by Kozeny-Carman

The Kozeny-Carman equation is well known in fluid dynamics. Relatively better results for pressure drop are obtained when this model is applied to laminar flow. Liu [32] and Patel and Deheri [33] have suggested that the use of the Kozeny-Carman formula turns in the relation:

$$\psi = \frac{D_c^2 e^3}{72(1-e)^2}\frac{l}{l'} \tag{20}$$

where e is the porosity and l/l' is the length ratio. From experimental investigations the length ratio is proposed to be around 2.5 under suitable situations. Thus, the Kozeny-Carman formula takes the form:

$$\psi = \frac{D_c^2 e^3}{180(1-e)^2} \tag{21}$$

Resorting to the boundary conditions (19), the non-dimensional form of the pressure distribution in the case of Kozeny-Carman, is derived as:

$$P = (-6-6\tau+SA)\int_1^R \frac{R}{g(\bar{h})+A}dR + \frac{S}{10}(3\Omega_f^2+4\Omega_f+3)\int_1^R \frac{Rg(\bar{h})}{g(\bar{h})+A}dR \tag{22}$$

where:

$$g(\bar{h}) = \bar{h}^3 + 3\bar{h}^2\bar{\alpha} + 3(\bar{\sigma}^2+\bar{\alpha}^2)\bar{h} + 3\bar{\sigma}^2\bar{\alpha} + \bar{\alpha}^3 + \bar{\varepsilon}$$

The non-dimensional load carrying capacity of the bearing system is determined from:

$$W = -\frac{h_0^3}{2\pi\eta a^4 \dot{h}_0}w = \int_0^1 RPdR$$

$$W = \left(3+3\tau-\frac{1}{2}SA\right)\int_0^1 \frac{R^3}{g(\bar{h})+A}dR - \frac{S}{20}(3\Omega_f^2+4\Omega_f+3)\int_0^1 \frac{R^3 g(\bar{h})}{g(\bar{h})+A}dR \tag{23}$$

2.2 A capillary fissures model

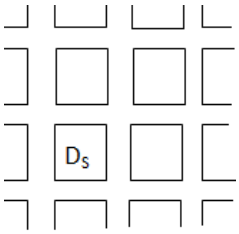

Fig. 3 Structure model of porous sheets given by Irmay

In Fig. 3, the model of porous sheets given by Irmay consists of three sets of mutually orthogonal fissures (a mean solid size D_S). Assuming no loss of hydraulic gradient at the junctions, Irmay [34] and Patel and Deheri [33] obtain permeability:

$$\psi = \frac{D_S^2\left(1-(1-e)^{\frac{2}{3}}\right)}{12(1-e)} \tag{24}$$

where e is porosity.

In view of the boundary conditions (19), the dimensionless pressure distribution for the Irmay model is found to be:

$$P = (-6-6\tau+SD)\int_1^R \frac{R}{g(\bar{h})+D}dR + \frac{S}{10}(3\Omega_f^2+4\Omega_f+3)\int_1^R \frac{Rg(\bar{h})}{g(\bar{h})+D}dR \tag{25}$$

The non-dimensional load carrying capacity is calculated as:

$$W = -\frac{h_0^3}{2\pi\eta a^4 \dot{h}_0}w = \int_0^1 RPdR$$

$$W = \left(3+3\tau-\frac{1}{2}SD\right)\int_0^1 \frac{R^3}{g(\bar{h})+D}dR - \frac{S}{20}(3\Omega_f^2+4\Omega_f+3)\int_0^1 \frac{R^3 g(\bar{h})}{g(\bar{h})+D}dR \tag{26}$$

3. Results and Discussions

The dimensionless pressure distribution is calculated from Eq. (22) and Eq. (25) while the non-dimensional load carrying capacity is determined from Eq. (23) and Eq. (26) for the Kozeny-Carman model and the Irmay one, respectively. It is obvious that the load carrying capacity increases by:

$$3\tau\int_0^1 \frac{R^3}{g(\bar{h})+A}dR$$

and:

$$3\tau\int_0^1 \frac{R^3}{g(\bar{h})+D}dR$$

as compared to the case of conventional lubricants.

It is observed from Eqs. (23) and (26) that the bearing can support a certain amount of load for both the models even when there is no flow. Setting the roughness parameters to be zero this discussion reduces to the effect of various porous structures on the Shliomis model based ferrofluid lubrication of a squeeze film between rotating curved circular plates. Also, considering the magnetization parameter to be zero this discussion turns out to the performance of different porous structures on a squeeze film in rotating curved circular plates (Bhat [27]). Further, in the absence of porosity this study reduces to the performance of a squeeze film in rotating curved circular plates. Lastly, taking curvature parameter to be zero, this is the effect of rotation on squeeze film performance as discussed in Wu [1].

It is clearly seen from Eqs. (23) and (26) that these expressions for non-dimensional load carrying capacity are linear with respect to magnetization parameter τ. Accordingly, increasing values of magnetization could lead to an increased load carrying capacity in the case of both the models.

The graphical representation of the results corresponding to the Kozeny-Carman model is shown in Figs. 4-18 while Figs. 19-33 account for the case of the Irmay model. From the graphical representation the following appears to be true,

1. A close glance suggests that the load carrying capacity is larger in the Kozeny-Carman model as compared to the Irmay one. Hence the former is more suitable for the Shliomis model based ferrofluid lubrication (Figs. 4, 5, 19, 20).

2. In increasing the load carrying capacity, the upper plate's curvature parameter has a dominant role to play. The increase in the load carrying capacity due to the upper plate's curvature parameter is bigger in the case of the Kozeny-Carman model as compared to the Irmay one (Figs. 5, 7, 8, 13, 14, 15, 20, 22, 23, 28, 29, 30).

3. The effect of $\bar{\psi}$ and ψ^* on the load carrying capacity with respect to τ is not that significant. The decrease in the load carrying capacity due to ψ^* is bigger in the case of the Irmay model. It is observed that there is a heavy reduction in the load carrying capacity due to ψ^* in the case of the Irmay model (Figs. 4, 6-12, 19, 21-27).

4. The reduction in the load carrying capacity due to porosity is higher in the case of Irmay (Figs. 6, 13, 21, 28).

5. Surprisingly, the decrease in the load carrying capacity due to the standard deviation is higher in the case of the Kozeny-Carman model (Figs. 9, 14, 16, 24, 29, 31).

6. Regarding the Irmay model the effect of skewness on the load carrying capacity with respect to ψ^* is not that significant as seen in Fig. 25. It can be noted that the positive skewness reduces the load carrying capacity while the load carrying capacity increases due to the negatively skewed roughness. It is easily observed that the trends of load carrying capacity with respect to variance is quite similar to that of skewness as can be seen in Figs. 18 and 33 (Figs. 10, 11, 15-18, 25, 30-33).

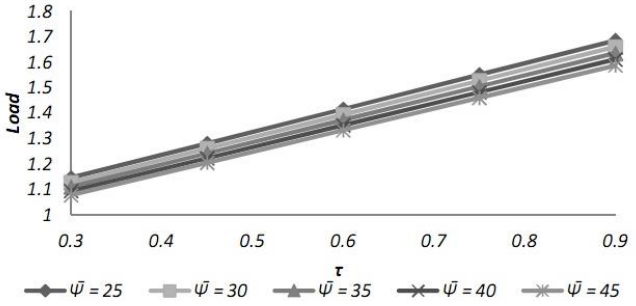

Fig. 4 Variation of load carrying capacity with respect to τ and $\bar{\psi}$

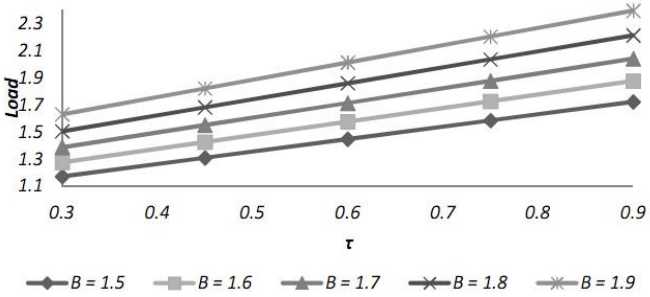

Fig. 5 Variation of load carrying capacity with respect to τ and B

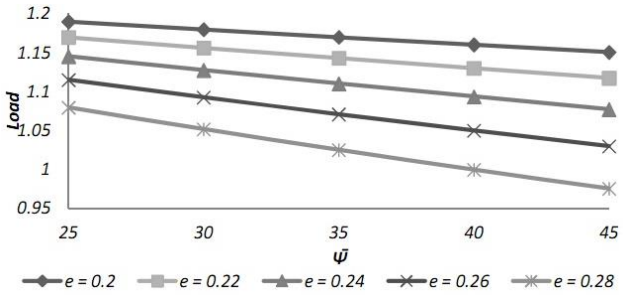

Fig. 6 Variation of load carrying capacity with respect to $\bar{\psi}$ and e

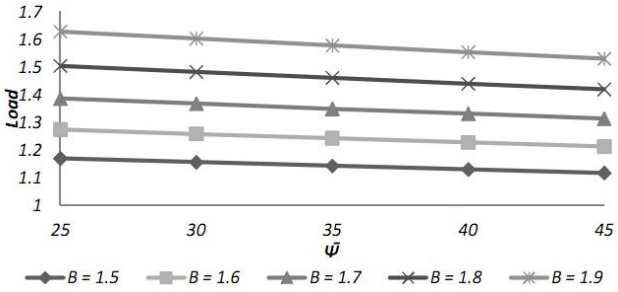

Fig. 7 Variation of load carrying capacity with respect to $\bar{\psi}$ and B

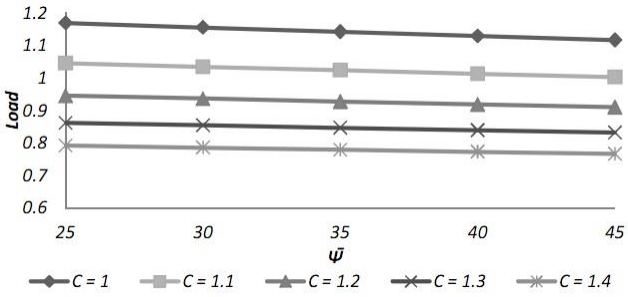

Fig. 8 Variation of load carrying capacity with respect to $\bar{\psi}$ and C

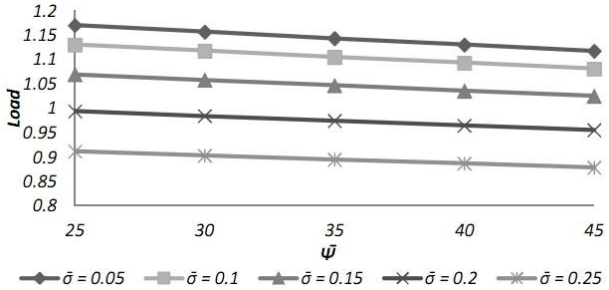

Fig. 9 Variation of load carrying capacity with respect to $\bar{\psi}$ and $\bar{\sigma}$

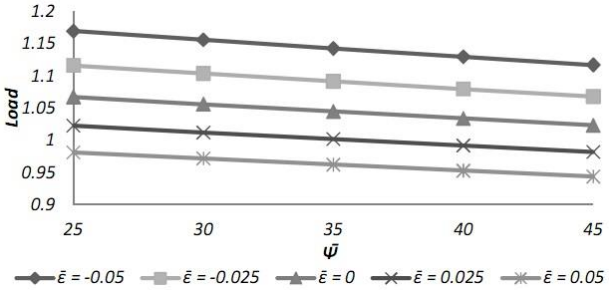

Fig. 10 Variation of load carrying capacity with respect to $\bar{\psi}$ and $\bar{\varepsilon}$

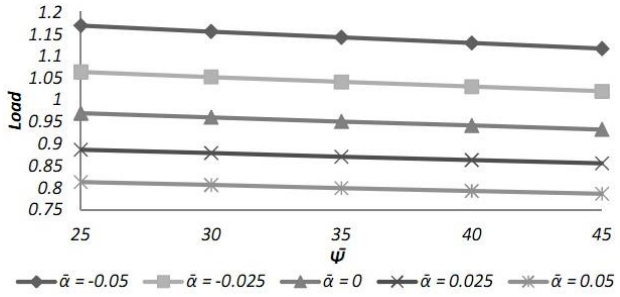

Fig. 11 Variation of load carrying capacity with respect to $\bar{\psi}$ and $\bar{\alpha}$

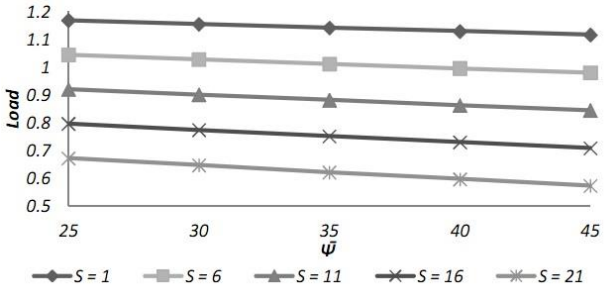

Fig. 12 Variation of load carrying capacity with respect to $\bar{\psi}$ and S

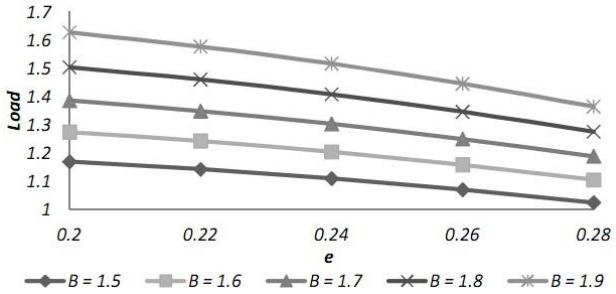

Fig. 13 Variation of load carrying capacity with respect to e and B

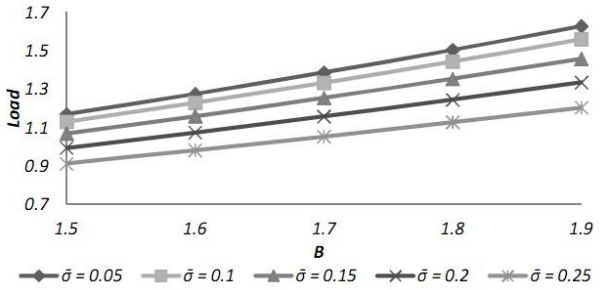

Fig. 14 Variation of load carrying capacity with respect to B and $\bar{\sigma}$

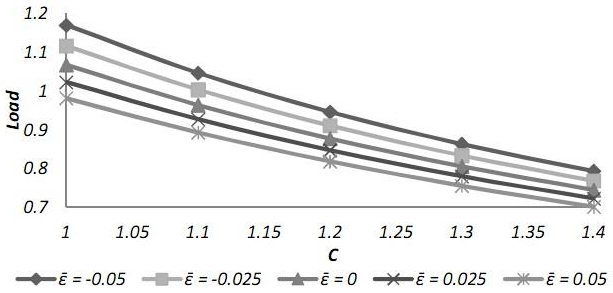

Fig. 15 Variation of load carrying capacity with respect to C and $\bar{\varepsilon}$

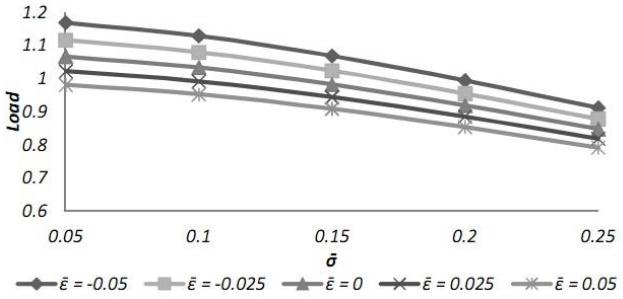

Fig. 16 Variation of load carrying capacity with respect to $\bar{\sigma}$ and $\bar{\varepsilon}$

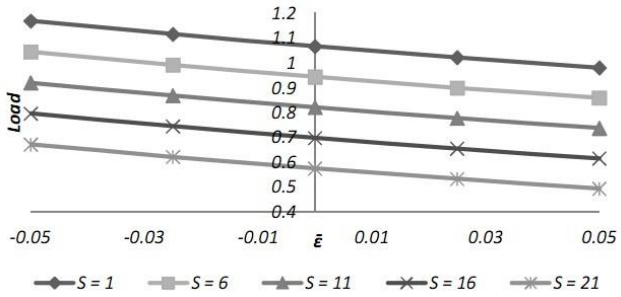

Fig. 17 Variation of load carrying capacity with respect to $\bar{\varepsilon}$ and S

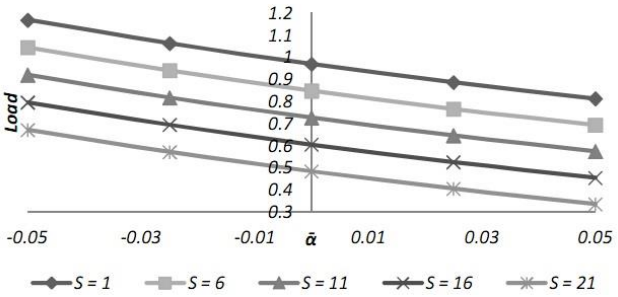

Fig. 18 Variation of load carrying capacity with respect to $\bar{\alpha}$ and S

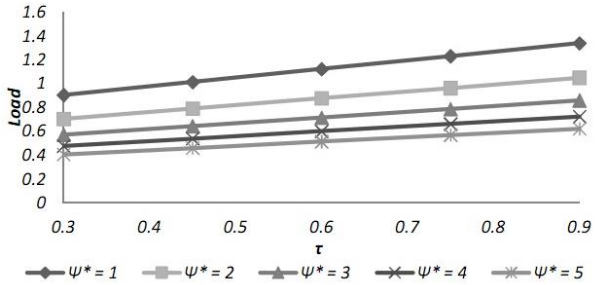

Fig. 19 Variation of load carrying capacity with respect to τ and ψ^*

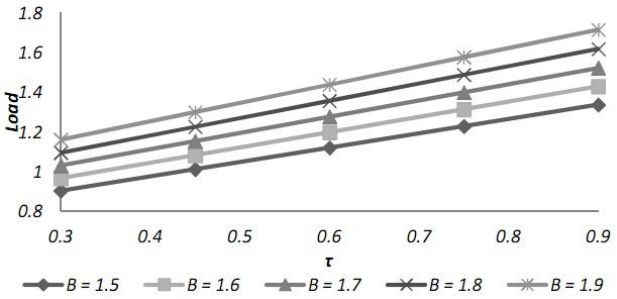

Fig. 20 Variation of load carrying capacity with respect to τ and B

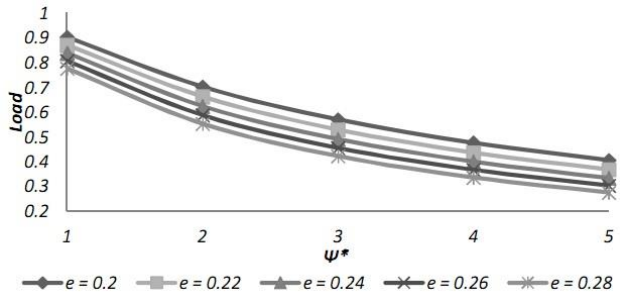

Fig. 21 Variation of load carrying capacity with respect to ψ^* and e

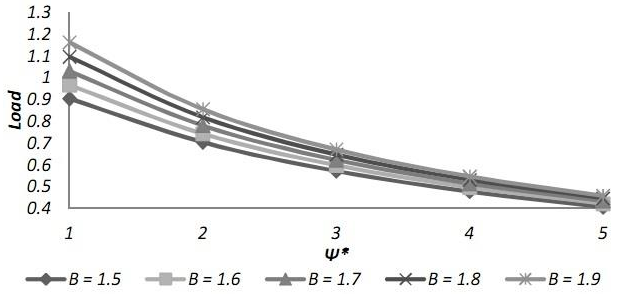

Fig. 22 Variation of load carrying capacity with respect to ψ^* and B

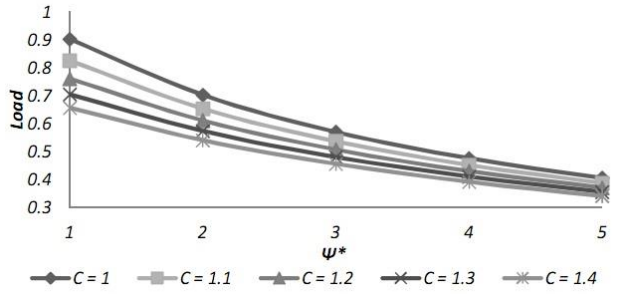

Fig. 23 Variation of load carrying capacity with respect to ψ^* and C

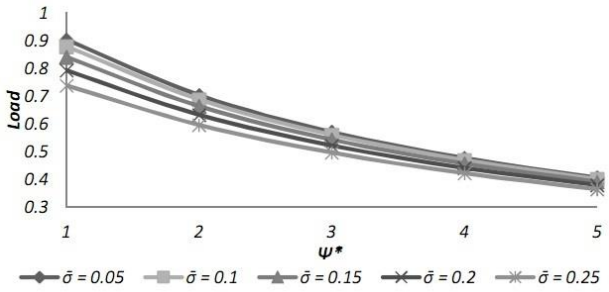

Fig. 24 Variation of load carrying capacity with respect to ψ^* and $\bar{\sigma}$

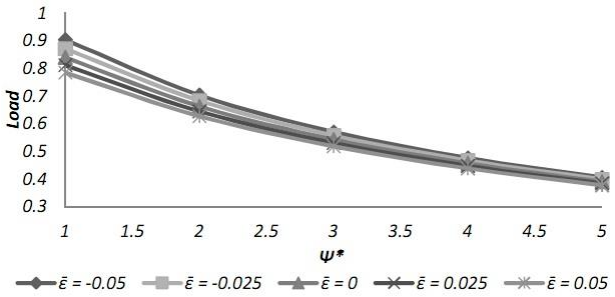

Fig. 25 Variation of load carrying capacity with respect to ψ^* and $\bar{\varepsilon}$

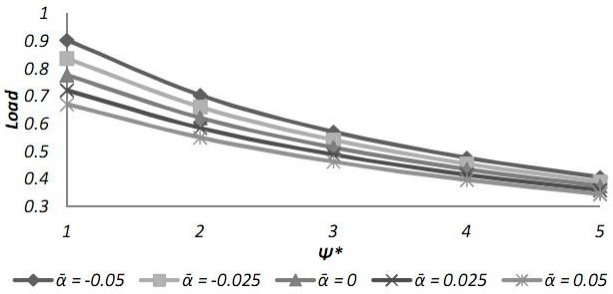

Fig. 26 Variation of load carrying capacity with respect to ψ^* and $\bar{\alpha}$

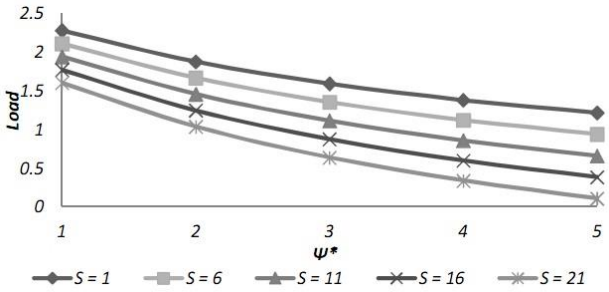

Fig. 27 Variation of load carrying capacity with respect to ψ^* and S

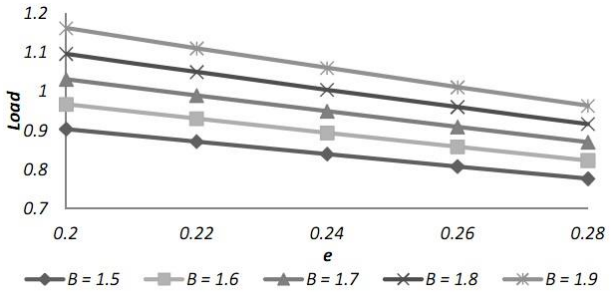

Fig. 28 Variation of load carrying capacity with respect to e and B

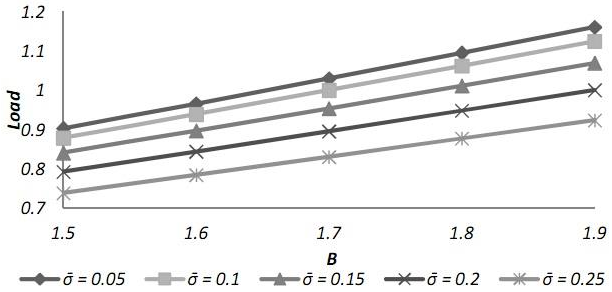

Fig. 29 Variation of load carrying capacity with respect to B and $\bar{\sigma}$

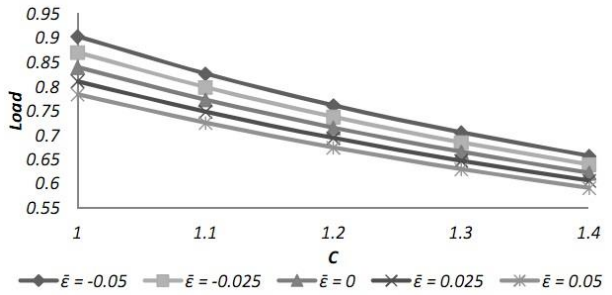

Fig. 30 Variation of load carrying capacity with respect to C and $\bar{\varepsilon}$

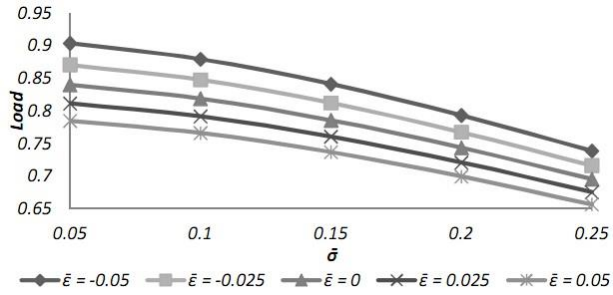

Fig. 31 Variation of load carrying capacity with respect to $\bar{\sigma}$ and $\bar{\varepsilon}$

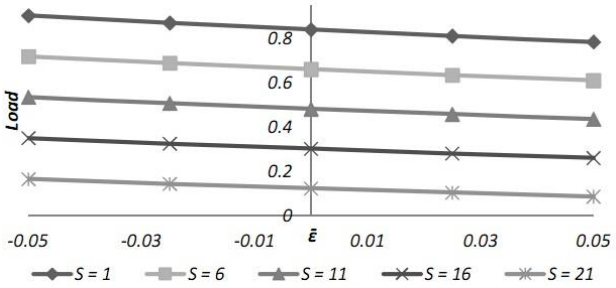

Fig. 32 Variation of load carrying capacity with respect to $\bar{\varepsilon}$ and S

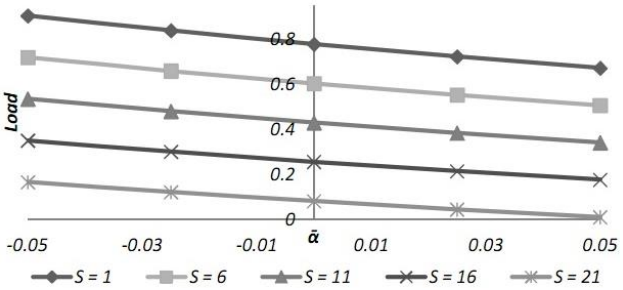

Fig. 33 Variation of load carrying capacity with respect to $\bar{\alpha}$ and S

A close look at the graphs tends to reveal that the adverse effect induced by standard deviation and porosity can be compensated, to a large extent, by the positive effect of magnetization and this compensation is relatively larger in the case of the Kozeny-Carman model. Further, the combined effect of magnetization and negatively skewed roughness goes a long way in minimizing the adverse effect of porosity, standard deviation and positive variance. The negative effect of rotation and porosity can also be reduced by a judicious choice of magnetization and curvature parameters when variance (-ve) is involved. It is found that the negatively skewed roughness causes an increase in the load-carrying capacity and gets raised by 5.88% more in the case of the Kozeny- Carman model. Lastly, it is revealed that there is at least 2.6% of increase in the load carrying capacity due to Shliomis model as compared to the Neuringer-Rosensweig one (Bhat [27]).

4. CONCLUSION

This investigation suggests that the roughness aspect must be taken into consideration while designing this type of bearing systems. The Kozeny-Carman model may be preferred over the Irmay one. In fact, magnetization plays a little role in improving the overall performance of the bearing system in the case of the Irmay model when the roughness is even moderate. Although there are several factors reducing the load carrying capacity, the bearing can support a good amount of load even in the absence of flow, which is far away from being true in the case of traditional lubricants. A suitable combination of magnetization, rotation ratio and curvature parameter may be more fruitful in the case of the Kozeny-Carman model.

REFERENCES

1. Wu, Hai, 1971, *The squeeze film between rotating porous annular disks*, Wear, 18(6) pp. 461-470.
2. Murti P.R.K., 1974, *Squeeze-Film Behavior in Porous Circular Disks*, Journal of Lubrication Technololgy, 96(2), pp. 206-209.
3. Vora, K.H., Bhat, M.V., 1980, *The Load capacity of a squeeze film between curved porous rotating circular plates*, Wear, 65, pp. 39-46.
4. Ram, Paras, Kumar, Vikas, 2012, *Ferrofluid flow with magnetic field-dependent viscosity due to rotating disk in porous medium*, International Journal of Applied Mechanics, 4(4), pp. 1250041-58.
5. Verma, P.D.S., 1986, *Magnetic fluid-based squeeze film*, International Journal of Engineering Science, 24(3), pp. 395-401.
6. Lu, R.F., Chien, R.D., Lin, J.R., 2006, *Effects of fluid inertia in magneto-hydrodynamic annular squeeze films*, Tribology International, 39(3), pp. 221-226.
7. Hsu, C.H., Lai, C., Hung, C.R., Lin, J.R., 2008, *Magneto-hydrodynamic squeeze film characteristics between circular discs including rotational inertial effects*, Proceedings of the Institution of Mechanical Engineers, Part J: Journal of Engineering Tribology, 222(2), pp. 157-164.
8. Zueco, Joaquín, Bég, O. Anwar, 2010, *Network numerical analysis of hydromagnetic squeeze film flow dynamics between two parallel rotating disks with induced magnetic field*, Tribology International, 43(3), pp. 532-543.
9. Huang, W., Cong, S., Liao, S., 2011, *Study of the ferrofluid lubrication with an external magnetic field*, Tribology Letters, 41, pp. 145-151.
10. Patel, J.R., Deheri, G.M., 2013, *Shliomis Model Based Ferrofluid Lubrication of Squeeze Film in Rotating Rough Curved Circular Disks with Assorted Porous Structures*, American Journal of Industrial Engineering, 1(3), pp. 51-61.
11. Ting, L.L., 1972, *A Mathematical Analog for Determination of Porous Annular Disk Squeeze Film Behavior Including the Fluid Inertia Effect*, J. Basic Eng., 94(2), pp. 417-421.
12. Wu, Hai, 1978, *A review of porous squeeze films*, Wear, 47(2), pp. 371-385.
13. Bhat, M.V., Deheri, G.M., 1991, *Squeeze film behaviour in porous annular discs lubricated with magnetic fluid*, Wear, 151(1), pp. 123-128.
14. Bhat, M.V., Deheri, G.M., 1993, *Magnetic-fluid-based squeeze film in curved porous circular discs*, Journal of Magnetism and Magnetic Materials, 127(1–2), pp. 159-162.
15. Elsharkawy, A.A., Nassar, M.M., 1996, *Hydrodynamic lubrication of squeeze-film porous bearings*, Acta Mechanica, 118(1-4), pp. 121-134.
16. Gupta J.L., Deheri, G.M. 1996, *Effect of roughness on the behavior of squeeze film in a spherical bearing*, Tribology Transaction, 39, pp. 99-102.
17. Deheri, G.M., Patel, R.M., Abhangi, N.D., 2010, *Magnetic fluid based squeeze film between transversely rough curved plates*, Advanced Tribology(Proceedings of CIST2008 & ITS-IFToMM2008), pp. 54-55.
18. Basti, D.P., 2013, *Effect of surface roughness and couple stress on squeeze films between curved annular plates*, ISRN Tribology, 2013, Article Id 640178.
19. Prakash, J., Tiwari, K., 1983, *Roughness effects in porous circular squeeze-plates with arbitrary wall thickness*, Journal of Lubrication Technology, 105, pp. 90-95.
20. Deheri, G.M., Patel, H.C., Patel, R.M., 2007, *Behaviour of magnetic fluid based squeeze film between porous circular plates with porous matrix of variable thickness*, International Journal of Fluid mechanics, 34(6), pp. 506-514.
21. Vadher, P.A., Vinodchandra, P.C., Deheri, G.M., Patel, R.M., 2008, *Behaviour of hydromagnetic squeeze film between two conducting rough porous circular plates*, Journal of Engineering Tribology, 222 (part J), pp. 569-579.
22. Patel, J.R., Deheri, G.M., 2013, *Shliomis model based magnetic fluid lubrication of a squeeze film in rotating rough curved circular plates*, Caribbean Journal of Science and Technology, 1, pp. 138-150.
23. Patel, J.R., Deheri, G., 2014, *Shliomis model-based magnetic squeeze film in rotating rough curved circular plates: a comparison of two different porous structures*, Int. J. Computational Materials Science and Surface Engineering, 6(1), pp. 29–49.
24. Christensen, H., Tonder, K.C., 1969, *Tribology of rough surfaces: stochastic models of hydrodynamic lubrication*, SINTEF, Report No. 10, pp. 69-18.
25. Christensen, H., Tonder, K.C., 1969, *Tribology of rough surfaces: parametric study and comparison of lubrication models*, SINTEF, Report No. 22, pp. 69-18.

26. Christensen, H., Tonder, K.C., 1970, *The hydrodynamic lubrication of rough bearing surfaces of finite width*, ASME-ASLE Lubrication Conference, Cincinnati. OH. Paper no. 70-lub-7.
27. Bhat, M.V., 2003, *Lubrication with a Magnetic fluid*, India: Team Spirit (India) Pvt. Ltd.
28. Abhangi, N.D., Deheri, G.M., 2012, *Numerical modeling of squeeze film performance between rotating transversely rough curved circular plates under the presence of a magnetic fluid lubricant*, ISRN Mechanical Engineering, 2012, Article ID 873481.
29. Shliomis, M. I., 1972, *Effective viscosity of magnetic suspensions*, Sov. Physics JETP., 34, pp. 1291-1294.
30. Prajapati, B.L., 1995, *On Certain Theoretical Studies in Hydrodynamic and Electro-magneto hydrodynamic Lubrication*, PhD thesis, S.P. University, Vallabh Vidyanagar, Gujarat, India.
31. Deheri, G.M., Andharia, P.I., Patel, R.M., 2005, *Transversely rough slider bearings with squeeze film formed by a magnetic fluid*, International Journal of Applied Mechanics and Engineering, 10(1), pp. 53-76.
32. Liu, J., 2009, *Analysis of a porous elastic sheet damper with a magnetic fluid*, Journal of Tribology, 131, pp. 0218011-15.
33. Patel, J.R., Deheri, G.M., 2013, *A comparison of porous structures on the performance of a magnetic fluid based rough short bearing*, Tribology in industry, 35(3), pp. 177-189.
34. Irmay, S., 1955, *Flow of liquid through cracked media*, Bull. Res. Counc. Isr, 5A(1), pp. 84.

DEJSTVO RAZNIH POROZNIH STRUKTURA NA PODMAZIVANJE GVOZDENIM FLUIDOM, ZASNOVANO NA ŠLIOMISOVOM MODELU, FILMA STISNUTOG IZMEĐU OBRTNIH HRAPAVIH ZAKRIVLJENIH PRSTENASTIH PLOČA

U radu su prikazana nastojanja da se analizira podmazivanje gvozdenim fluidom, zasnovano na Šliomisovom modelu, filma stisnutog između obrtnih hrapavih zakrivljenih ploča pri čemu gornja ploča ima poroznu površinu. Obrađeni su različiti modeli poroznosti. Primenjen je stohastički model Kristensena i Tondera za procenu dejstva površinske hrapavosti. Numerički je rešena s tim povezana stohastički usrednjena jednačina Rejnoldsovog tipa za dobijanje distribucije pritiska što dovodi do izračunavanja nosivosti. Grafički prikaz rezultata pokazuje da je Kozeni-Karmanov model mnogo povoljniji u poređenju sa Irmejevim sa projektantskog stanovišta. Takođe se pokazalo da podmazivanje gvozdenim fluidom, po Šliomisovom modelu, relativno bolje deluje od Nojringer-Rosensvajgovog. Iako ležaj trpi zbog poprečne površinske hrapavosti, odgovarajućim izborom parametra zakrivljenosti i koeficijenta obrtanja, negativno dejstvo poroznosti i standardna devijacija se mogu smanjiti na minimum podmazivanjem gvozdenim fluidom, barem u slučaju negativno zakošene hrapavosti.

Ključne reči*: stisnuti film, zakrivljene prstenaste ploče, hrapavost, magnetni fluid, obrtanje, porozne strukture*